Birthdate aligns vestibular sensory neurons with central and motor partners across a sensorimotor reflex circuit for gaze stabilization

Stephanie Huang[1,2] **Marie R. Greaney**[1] **Samantha N. Davis**[1] **David Schoppik**[1] **Dena Goldblatt**[1,2,3,*]
[1]Depts. of Otolaryngology, Neuroscience & Physiology, and the Neuroscience Institute, NYU Grossman School of Medicine
[2]Center for Neural Science, New York University
[3]Lead Contact
[*]Correspondence: goldblatt.dena@gmail.com

Developing populations of connected neurons often share spatial and/or temporal features that anticipate their assembly. A unifying spatiotemporal motif might link sensory, central, and motor populations that comprise an entire circuit. In the sensorimotor reflex circuit that stabilizes vertebrate gaze, central and motor partners are paired in time (birthdate) and space (dorso-ventral). To determine if birthdate and/or dorso-ventral organization could align the entire circuit, we measured the spatial and temporal development of the sensory circuit node: the vestibular ganglion neurons. We discovered progressive dorsal-to-ventral development in the vestibular ganglion that diverges from its functional (rostrocaudal) organization. With an acute optical lesion and calcium imaging paradigm, we found that this common spatiotemporal axis anticipated functional sensory-to-central partner matching. We propose a "first-come, first-served" model in which birthdate organizes the sensory, central, and motor populations that comprise the gaze stabilization circuit. Our work suggests a general means for poly-synaptic circuit assembly across embryonically-diverse neural populations.

INTRODUCTION

Neural circuit elements develop in both space and time. During development and maturation, spatial relationships among somata and/or neuropil impose structural constraints on neural circuit assembly and function[1–5], leaving a topographic record[6–8]. Complementarily, progressive neurogenesis is correlated with spatial map formation and subsequent synaptic partner matching[9], such that circuit nodes assemble in time[10–18]. While matching of partner populations of neurons in space and time is well-established, sensorimotor circuits are almost all poly-synaptic. Further, sensorimotor circuits generally span embryologically-diverse tissue, opening the question of whether the spatial and temporal features that pair partners might similarly organize an entire circuit.

The vertebrate vestibulo-ocular reflex is a canonical sensorimotor circuit that uses precise sensory-to-motor partner matching to stabilize gaze. The circuit transforms two vertical directions of head/body destabilization (nose-up/nose-down) into compensatory eye rotation behavior (eyes-down/eyes-up). Anatomically, the circuit consists of hair cells in the inner ear, sensory afferents in the anterior (vestibular) statoacoustic ganglion, central vestibular projection neurons, motor neurons, and extraocular muscles[19]. Each direction of motion (up/down) is segregated into its own specific channel comprised of directionally-selective hair cells, neurons, and muscles. A small model vertebrate, the larval zebrafish, offers exceptional optical and genetic access to each population[20–22]. Further, the external development and anatomical simplicity of larval zebrafish[23] affords a unique opportunity to characterize sensorimotor circuit assembly.

Divergent organizational and functional axes exist between central/motor populations and the sensory periphery. Functional imaging of the vestibular ganglion establishes a rostrocaudal axis for nose-down/nose-up segregation, matched to the position of hair cells along the utricular macula[24], and electron micrographs of the vestibular periphery suggest that vestibular ganglion maturation proceeds along the mediolateral axis[25]. In contrast, the central and motor neuron partners are temporally and functionally aligned along the dorsoventral axis: early-born neurons are dorsally positioned and mediate nose-up/eyes-down behavior, while their late-born, ventral counterparts perform the converse (nose-down/eyes-up)[26,27]. Notably, differentiating sensory progenitors are pushed dorsally as they delaminate in the ventral otic floor[28], potentially decoupling functional topography from spatiotemporal development in the vestibular ganglion. Even still, dorsal vestibular ganglion neurons include both nose-up and nose-down subtypes[24,25], underscoring the point that circuit assembly cannot be solved using a "dorsal-to-dorsal" spatial map alone. We predicted that instead, time is the "missing" variable in peripheral vestibular development, and the complex task of poly-synaptic partner matching achieved simply by assembling neurons with common temporal availability.

Here, to determine if a single motif could anticipate separate up/down channels across the entire vestibulo-ocular reflex circuit, we studied the development of the sensory ganglion in space and time. Anatomical birthdating revealed that sensory neurons emerged along a dorsoventral axis, in contrast to their functional (rostrocaudal) axis. Bipolar afferent projections to peripheral and central targets followed patterns of somatic development. By coupling acute optical lesions with calcium imaging, we then discovered that early-born sensory neurons form functional connections with spatiotemporally-matched central neuron cohorts. Collectively, our findings support that the development of peripheral vestibular neurons, like their central and motor neuron counterparts, proceeds along a dorsoventral axis, where early-born neurons belong to a specific channel (nose-up). Our findings here complete the characterization of vestibulo-ocular reflex circuit development, revealing a unified spatiotemporal pattern to circuit assembly that spans peripheral sensory, central, and motor areas.

RESULTS

Tg(-6.7Tru.Hcrtr2:GAL4-VP16) provides reliable access to the vestibular statoacoustic ganglion neurons that mediate vertical gaze stabilization

In zebrafish, the vestibular sensory neurons that relay utricular pitch-tilt (nose-up/nose-down) sensation are located in the anterior statoacoustic ganglion ("vestibular ganglion")[29,30] (Figure 1A). Past developmental studies used a transgenic line, *Tg(-17.6isl2b:GFP)*, that labels the statoacoustic ganglion with a fluorescent reporter driven by the *isl2b* promoter[28,31–34]. However, this line does not permit tagging subsets of neurons across development[22].

We instead leveraged the *Tg(-6.7Tru.Hcrtr2:GAL4-VP16)* transgenic line[20,35] which labels a population of neurons whose location is consistent with the vestibular ganglion[30] and that co-localize with *Tg(-17.6isl2b:GFP)* (Figure 1B). To evaluate how efficiently and reliably *Tg(-6.7Tru.Hcrtr2:GAL4-VP16)* labels these neurons, we mapped their spatial location to a *Tg(-17.6isl2b:GFP)* reference framework at 5 days post-fertilization (dpf) (Figures 1C to 1F, Methods), when vertical vestibulo-ocular reflex circuit anatomy is stable[20] and behavior is directionally appropriate[36,37]. Labeled neurons in both lines spanned approximately 60 µm in the dorsoventral and mediolateral axes, and 70 µm in the rostrocaudal axis. *Tg(-6.7Tru.Hcrtr2:GAL4-VP16)* expression covered same spatial extent of the vestibular ganglion as *Tg(-17.6isl2b:GFP)* (dorsoventral: $p_{KS\ test}$=0.76; rostrocaudal: $p_{KS\ test}$=0.78; mediolateral: $p_{KS\ test}$=0.99) (Figure 1G) and at a comparable density (median, *isl2b*: 73±12 neurons/hemisphere; median, *-6.7Tru.Hcrtr2* 77±15 neurons/hemisphere; $p_{rank\ sum\ test}$=0.79) (Figure 1H). We conclude that *Tg(-6.7Tru.Hcrtr2:GAL4-VP16)* provides reliable access to the vestibular sensory neurons that relay utricular-mediated tilt sensation.

Developmental time organizes a dorsoventral map in the vestibular ganglion

To tag vestibular ganglion neurons during development, we used *Tg(-6.7Tru.Hcrtr2:GAL4-VP16)* to express a photoconvertible reporter, Kaede[38], that enables permanent optical labeling of experimenter-defined temporal cohorts[26,27,39]. We tagged cohorts of neurons born at intermediate stages between 22–72 hours post-fertilization (hpf) (Figure 2A), the timecourse over which the vestibular ganglion differentiates in larval zebrafish[28,40]. We imaged tagged vestibular ganglion neurons at 5 dpf. Tagged neurons (i.e., born before the time of Kaede photoconversion) were readily identifiable by the presence of red, converted Kaede; neurons born after conversion contained only green, unconverted protein (Figure 2B). The number of tagged neurons increased linearly from 22–72 hpf (N=5 converted larvae/timepoint; Figure 2C, Table 1). Most neurons (82% of control) evaluated at 5 dpf were born by 72 hpf, in line with prior reports of *isl2b*+ differentiation in the larval vestibular ganglion[28].

Next, we examined how organization within the vestibular ganglion emerges. We first evaluated the location of two cohorts: the earliest- (before 26 hpf) and latest-born (after 48 hpf), collectively comprising half (55%) of all vestibular ganglion neurons (Table 1). Strikingly, these cohorts were differentially organized along the dorsoventral axis (Figure 2D). We quantified the probability of observing early- and late-born soma in each spatial axis (Figure 2E). Early and late cohort position was significantly different along the dorsoventral ($p_{KS\ test}=1.1\times10^{-16}$) and rostrocaudal axes ($p_{KS\ test}=1.7\times10^{-4}$). The early-born cohort was caudal of center relative to control ($p_{KS\ test}=1.0\times10^{-10}$). Mediolateral organization was not observed ($p_{KS\ test}$=0.25).

Dorsal and ventral cohorts could be born in discrete temporal windows or continuously across time. Evidence that dorsal neurons continue to accumulate at later developmental stages would support the latter. To differentiate these hypotheses, we evaluated the location of neurons born before (Figure 3A) and after (Figure 3B) all seven of our converted timepoints (N=5 larvae/cohort; full statistics in Table 2). The dorsal bias we observed persisted until approximately 36 hpf (36 hpf vs. 33 hpf: $p_{ANOVA\ multiple\ comparisons\ test}$=0.20; Figure 3C). Qualitatively, by 48 hpf, nearly all "born after" neurons were located ventral to the midpoint of the ganglion (Figure 3B). We interpret that dorsal and ventral neurons are largely born in opposing temporal windows, offset by approximately 8–12 hours: dorsal neurons from 22–48 hpf, and ventral neurons from 30–72 hpf.

The dorsoventral accumulation we observed is intriguing given that nose-up and nose-down subtypes of vestibular ganglion neurons are topographically organized into rostral (down) and caudal (up) functional domains[24,25]. As the earliest-born 25% of the vestibular ganglion lies caudal of center (Figure 2E), we next asked if functional topography followed ganglion development. We evaluated the rostro-caudal distribution of neurons at each stage relative to the ganglion midpoint. The exclusive caudal bias to early-born neurons was abrogated by 30 hpf (Figure 3A), when rostral neurons first became apparent. After 33 hpf, rostral and caudal neurons emerged contemporaneously (33 hpf vs. 30 hpf: $p_{ANOVA\ multiple\ comparisons\ test}$=0.94, Figure 3D, Table 2). Both caudal and rostral neurons remained undifferentiated after 60 hpf (Figure 3B). While our dataset contains a low number of undifferentiated neurons at 72 hpf, the presence of rostral neurons at this age suggests that — unlike their dorsal counterparts — ventro-rostral and ventro-caudal accumulate continuously through late developmental stages.

We conclude that after 30 hpf, rostrocaudal development is not a significant predictor of functional organization. Instead, dorsoventral development is the primary axis for vestibular ganglion accumulation.

Bipolar afferent organization follows spatial patterns of somatic development

Somatic topography anticipates axonal connectivity[2,26,41,42]. Vestibular ganglion neurons send bipolar afferents ventrally to peripheral hair cells in the utricular macula and dorsally to central hindbrain targets via the VIIIth nerve[25,29] (Figures 4A and 4B). We hypothesized that the orderly positioning of early-born vestibular ganglion neurons could spatially constrain the path of their projections within each bipolar afferent bundle. We therefore analyzed the bipolar afferents of the converted neurons described previously (Figure 4C) along its width (rostrocaudal axis). We evaluated the spatial distribution of converted axons (i.e., from neurons born before the time of conversion) at 5 dpf, reasoning that organization at 5 dpf reflects how axons become assembled into the VIIIth nerve.

We first evaluated peripheral projections to the utricular macula (Figures 4D and 4E; N=3 hemispheres/timepoint). Converted axons from soma born before 22 hpf were only observed in the caudal macula ("born before" vs. all fluorescence, rostrocaudal axis: $p_{KS\ test}=5.3\times10^{-11}$). Conversion spread rostrally by 30 hpf and spanned the full rostrocaudal extent of the macula by 36 hpf ($p_{KS\ test}=0.50$), matching the temporal emergence of rostrally-positioned somata. Next, we evaluated projections to the VIIIth nerve (Figures 4F and 4G; N=3 hemispheres/timepoint). In the caudal half of the axon bundle, we observed a faint but visible converted axon from soma born before 22 hpf. We observed stronger conversion in the caudal and center of the axon bundle from somata born before 26 hpf ($p_{KS\ test}=0.016$). As with the macula, rostral spread across the VIIIth nerve bundle was evident by 30 hpf ($p_{KS\ test}=0.69$). Together, we conclude that rostrocaudal organization within the utricular macula and VIIIth nerve follows neuronal birthdate: early-born soma (caudal) project caudally or center-caudally within each axon bundle, respectively.

Early-born vestibular ganglion neurons assemble with spatiotemporally- and functionally-matched central neuron cohorts

Vestibular ganglion neurons relay tilt sensation to central (hindbrain) projection neurons in the tangential nucleus[25,26], which are necessary and sufficient for vertical (nose-up/nose-down) gaze stabilization behavior[20,36]. In a prior study, we found that both birthdate and function segregate central vestibular neurons: early-born dorsal neurons are sensitive to nose-up tilts, and late-born ventral neurons are sensitive to nose-down tilts[26]. This pattern mirrors the dorsoventral development we observed for their vestibular ganglion inputs and occurs over a comparable temporal window (22–48 hpf)[26]. Does birthdate anticipate synaptic assembly between partner populations across the developing vestibulo-ocular reflex circuit? We predicted that the earliest-born vestibular ganglion neurons (dorsal, caudal, nose-up) would assemble with temporally- (early-born), spatially- (dorsal), and functionally- (nose-up) matched central neuron targets (Figure 5A).

We first evaluated whether vestibular ganglion afferents from early-born neurons are anatomically poised to wire to temporally-matched central targets. At 5 dpf, VIIIth nerve input from neurons born before 22 hpf exclusively targeted the early-born (dorsal) tangential nucleus (Figure 5B). The matched connectivity suggests that early-born vestibular ganglion neurons innervate commonly positioned central neuron partners. However, *Tg(-6.7Tru.Hcrtr2:GAL4-VP16)* labels other cranial sensory ganglia that differentiate comparably early with axons that project along the VIIIth nerve[32]. Therefore, we cannot conclude from anatomical observations alone that early-arriving sensory input exclusively derives from the vestibular ganglion.

Next, we evaluated whether early-born neurons in the vestibular ganglion and tangential nucleus are functionally connected. We used an acute optical lesion and calcium imaging paradigm (Figure 5C). First, we birthdated larvae at 26 hpf to tag the earliest-born 20% of the vestibular ganglion. Lesion of these early-born neurons was not technically feasible due to their close proximity to the dorsal VIIIth nerve bundle and local vasculature. Instead, at 5 dpf, we unilaterally lesioned the 80% of vestibular ganglion neurons born after 26 hpf (Figures 5D and 5E), leaving only the early-born (dorso-caudal, nose-up) neurons available to relay tilt sensation. To evaluate changes in central neuron responses to tilt sensation, we used Tilt-In-Place Microscopy (TIPM)[43]. Briefly, TIPM reports changes in a genetically-encoded calcium indicator, GCaMP6s[44], in central neurons after delivering nose-up and nose-down pitch tilts (Figure 5F). At 5 dpf, the vestibular ganglion is the primary source of our pitch tilt stimulus input to these central neurons[26]. Therefore, loss of central neuron responses to tilt sensation should directly reflect loss of corresponding statoacoustic ganglion input.

We predicted that loss of late-born (ventral) vestibular ganglion inputs would eliminate pitch tilt responses in spatiotemporally-matched (late-born, ventral, nose-down) central neurons. We imaged the tilt responses of n=172 tangential nucleus neurons from N=4 control hemispheres and n=115 neurons from N=4 hemispheres with acute, unilateral vestibular ganglion lesion. We observed a substantial reduction in the number of tilt-responsive neurons (median control: 89.4±6.0% responsive; lesion: 36.9±21.4% responsive; $p_{rank\ sum\ test}=0.03$), driven by a near total loss of responses to nose-down tilts (nose-down: median control, n=15±4 neurons/fish; lesion: n=1±2 neurons/fish; $p_{rank\ sum\ test}=0.03$; nose-up: control, n=17±2 neurons/fish; lesion: n=10±5 neurons/fish; $p_{rank\ sum\ test}=0.09$; Figure 5G). As nose-down neurons are in the ventral tangential nucleus[26], we expected to see a corresponding loss of responses in ventral neurons. Central neurons that remained able to respond to tilt sensation were, in fact, dorsally-shifted (median position: control, 25±8μm; lesion, 30±7μm, $p_{KS\ test}=0.01$; Figures 5H to 5J). We interpret the absence of tilt responses in the ventral tangential nucleus to be a direct consequence of loss of late-born (ventral) vestibular ganglion inputs. Correspondingly, the preservation of dorsal (nose-up) central neuron responses suggests a tight matchup in time between early-born (dorso-caudal, nose-up) vestibular ganglion neurons and their early-born (dorsal, nose-up) targets.

Collectively, these experiments demonstrate early-born vestibular ganglion neurons assemble with spatiotemporally-matched central neuron targets.

DISCUSSION

Here, we studied the development of topography in the vestibular ganglion. Unlike its rostro-caudal functional organization, we discovered that the development of the vestibular ganglion proceeds along a dorsal-to-ventral axis. Intriguingly, this dorsal/early organizational motif is shared across the entire sensorimotor circuit for gaze stabilization (Figure 6). Afferents from the vestibular ganglion systematically target the utricle across development, and axon position in the VIIIth nerve follows an orderly spatial progression. Finally, our loss-of-function experiments establish that early-born cohorts of peripheral sensory neurons preferentially assemble with early-born central neuron partners, just as early-born central neurons assemble with early-born motor neuron targets[26]. Taken together, our work reveals that the vertical vestibulo-ocular reflex circuit assembles sequentially in time, aligning sensory, central, and motor output neurons into separate up and down channels. Our findings speak to the earliest steps in construction of an ancient and conserved sensorimotor reflex circuit.

Implications for understanding the organization and specification of vestibular ganglion subtypes

The temporal structure we observed in the vestibular ganglion reconciles a disconnect between past studies of progenitor development[28,33] and the "mature" topography of the post-mitotic ganglion[24,25]. Prior work parsed the statoacoustic ganglion into coarse anteroposterior domains by sensory input modality (auditory vs. vestibular)[28,29], providing a broad framework to discover corresponding anteroposterior patterns of progenitor delamination[28,33,45–48], molecular differentiators[29,49–53], and VIIIth nerve organization by sensory ganglia origin[32,54,55]. Within the anterior (vestibular) ganglion, recent advances in connectomic and optical imaging revealed that rostral neurons preferentially represent nose-down stimuli, and caudal neurons nose-up[24,25]. Here, the temporal structure we uncovered suggests these spatial patterns are uncoupled from vestibular ganglion birthdate. Instead, vestibular ganglion development may be more closely influenced by the spatial pressures imposed by sequential patterns of progenitor delamination: differentiated statoacoustic ganglion neurons are pushed dorsally by their transit-amplifying precursors in the ventral otic floor[28], leading to the dorsal-to-ventral accumulation of neurons we observed within the ganglion. Future studies could test these hypotheses by tracking the migration patterns of the same vestibular ganglion neurons across development and life[56], as recent work tracked progenitor migration linked to coarse (anteroposterior) ganglion domain formation[33].

Early/late temporal cohorts in the vestibular ganglion may have unique functional dynamics. Individual vestibular ganglion neurons can receive inputs from either extrastriolar (low frequency, ipsilateral roll) input or striolar (high frequency, contralateral roll) hair cells. Earlier connectomic work inferred based on estimated age that striolar/extrastriolar innervation develops along a mediolateral axis[25]. However, we did not observe mediolateral changes in birthdate. As we imaged the vestibular ganglion from a lateral view, our mediolateral resolution may have simply been insufficient. Thus, our data is not necessarily incompatible with mediolateral maturation. Alternatively, the connectomic data is based on a single hemisphere from one fish, and neuronal age must be inferred. Together, the temporal organization of the vestibular ganglion may provide molecular access to distinct input channels — of broad importance given the general susceptibility of the vestibular periphery in disease[57]. Although it is not achievable with TIPM, functional imaging of birthdated neurons in the vestibular ganglion would be possible with the rotatable microscope in[24,58]. Future work may therefore resolve the axes along which functional development of the vestibular ganglion proceeds.

Fate and connectivity in the vestibulo-ocular reflex circuit: Destined by time?

How might structural connectivity in the vestibulo-ocular reflex circuit emerge in time? Our model predicts that time reduces the complex task of matching synaptic partners across the peripheral and central nervous system to the passive assembly of first-available neurons, aligned across a common positional template. Key support comes from our finding that, as in other species[28,59–64], across the zebrafish vestibulo-ocular reflex circuit, dorsal-to-ventral neurogenesis[26,27] proceeds over a shared temporal window (24–48 hpf)[26–28]. In spinal reflex circuits[1,2,18], such parallel neurogenesis imposes temporal and/or spatial constraints on axon targeting. Unlike in these circuits, sensory and central partner populations in the vestibulo-ocular reflex circuit derive from different embryological precursors with distinct environmental pressures[40], posing additional complexity to partner matching. Previously, we established that early-born, dorsally-located central vestibular neurons in the hindbrain preferentially wire to early-born, dorsally-located motor neurons in the mid- and hindbrain[26]. Here we show that early-born dorsally-located neurons in the peripheral statoacoustic ganglion preferentially wire to early-born dorsally-located neurons in the hindbrain. Our findings support past proposals that neuronal position – a consequence of birthdate – pre-configures connectivity in the vestibulo-ocular reflex circuit[65]. A "first-come, first-served" mechanism to match temporally-available partners offers a simple means of poly-synaptic sensorimotor circuit construction.

Past work suggests that the true "first arriving" partners in the vestibulo-ocular reflex circuit are their peripheral sensory inputs. In zebrafish, hair cells in the utricular periphery become anatomically mature[52] and mechanically active[66,67] as neurogenesis is only just beginning in central/motor neurons[26,27]. Similar timelines have, again, been reported in zebrafish[28,32,40,68], avians[69], and mammals[70]. Together, these findings support emerging evidence[26,27,71,72] that the initial synaptic architecture of the vestibulo-ocular reflex circuit develops in the anterograde (sensory-to-motor) direction. Peripheral targets can influence the development of proprioceptive spinal pathways in a similar manner[73–77].

Curiously, though central axons project to motor targets soon after neurogenesis, synaptogenesis between central and motor neurons[26] and between motor neurons and muscles[71] is delayed until after differentiation across all vestibulo-ocular reflex populations is nearly complete. We propose that the early formation of sensory-central connections instructs downstream wiring specificity. Evidence that vestibular ganglion axons project soon after differentiation, and that sensory-central synaptogenesis proceeds during the downstream synaptogenesis "delay" would strongly support an anterograde assembly model of vestibulo-ocular circuit development.

While our model predicts that temporal availability allows early-to-early born cohorts to assemble, additional forces may still refine connectivity for late-born cohorts and as circuit function matures[37]. Though early input to the vestibulo-ocular reflex is exclusively nose-up (caudal), input after 30 hpf contains both up (dorso-caudal) and down (dorso-rostral) channels[24,25] that may project to similar (early/dorsal) central targets. This mismatch is puzzling given that these central projection neurons do not show strict nose-up selectivity until later[26,37]. We hypothesize that central projection neurons may initially receive input from both directionally-tuned channels during development. We predict that inappropriate (nose-down) sensory inputs are pruned at their dorsal central targets to enable directional selectivity in maturity. Notably, sensation is dispensable for vestibulo-ocular reflex circuit development[34,37,78], arguing against stimulus-driven remodeling[79,80] and in favor of molecular refinement[81]; Teneurin signaling has recently been shown to correct axon mis-sorting in such a manner[82]. Looking ahead, measuring when and how directional selectivity emerges in central neurons will be key to resolving the mechanisms for achieving synaptic specificity.

Temporal maps: a blueprint for neural circuit construction

Our findings link time with functional circuit assembly by discovering that time can shape spatial maps over relatively homogeneous functional scales, and across an entire poly-synaptic sensorimotor reflexive circuit. Across vertebrate and invertebrate models, the timing of neurogenesis regulates partner availability by constraining anatomical connectivity[26,45,83–88], function in local ensembles[89–91], and assembly into behaviorally-separable circuits[10,11,13,15–18,25,55,92]. Here we observed that time can also organize closely-related, binary subtypes of neurons (nose-up/nose-down) that subserve just one sensory modality (balance) and motor behavior (eye movements). Despite the clear structural constraint that time imposes on developing sensorimotor circuits, the extent to which individual systems may rely on passive "first-come, first-served" partner matching remains controversial[93,94]. The generalizability of our findings to other systems may be resolved in the future through transplantation experiments[93,94] or temporal manipulations[10]. More broadly, such experiments could reconcile whether there is one rule, such as "first-come first-served", or disparate rules that govern sensorimotor circuit assembly.

The continuity of the temporal map we discovered, from the sensory periphery to motor output, offers a path to resolve the extent to which the vestibulo-ocular reflex circuit is constructed holistically through shared codes or instead constructed as local modules[95], stitched together by local signals. One hypothesis is that shared organization, whether in space or time, reflects the existence of a shared molecular code that coordinates circuit assembly. Common, spatially-restricted patterns of chemorepulsive molecules underscore partner matching across retinal circuits[96–98]; can be spatially inverted across target populations[99]; and can even vary along spatial gradients, matching the graded functional tuning of synaptic partners[100]. However, the divergent embryological origins of each vestibulo-ocular reflex circuit populations suggests the nature of such a shared code is unlikely to be spatial, downstream of common extrinsic induction factors[41]. Instead, our temporal map predicts that "molecular matching" gradients might alternatively co-emerge in time. For example, time could establish "competency" windows in which neurons are maximally poised to respond to local wiring specificity signals[45,96,101–105], perhaps downstream of temporally-restricted transcription factor expression[10,87,88,94,106,107]. Emerging evidence supports that such temporal codes may be shared across related partner populations[108] and coarsely across brain regions[109], though whether these could act over relatively homogeneous scales remains unresolved. Early work predicted that "The basic connectivity scheme of the [vestibulo-ocular reflex circuit] is set up by determinate mechanisms of cell-cell recognition"[60], likely downstream of early fate specification programs[65,110]. Looking ahead, it will be illuminating to resolve whether this is achieved through distinct ligand-receptor pairs expressed in particular temporal cohorts or through just one factor, dynamically regulated or differentially available in time.

Conclusion

Here, we complete our characterization of shared spatial, temporal, and functional features across a developing sensorimotor reflex circuit. The common positioning of vestibular partner populations across developmental time is reminiscent of the shared topographic maps that align sensory space/body plans with central representations in canonical (i.e., retinal, auditory, somatotopic) sensory systems. For the vestibulo-ocular reflex circuit, temporal alignment may serve as a passive constraint on functional partner matching, simplifying assembly across diverse tissues. Though additional forces may subsequently refine connectivity as the vestibulo-ocular reflex circuit matures, our findings provide a key advance towards defining the initial structural blueprints that constrain the development of poly-synaptic reflex circuits.

MATERIALS AND METHODS

RESOURCE AVAILABILITY

KEY RESOURCES TABLE

Reagent or resource	Source	Identifier
Chemicals, peptides, and recombinant proteins		
Low melting point agarose	ThermoFisher Scientific	16520
Ethyl-3-aminobenzoic acid ethyl ester (MESAB)	Sigma Aldrich	E10521
Pancuronium bromide	Sigma Aldrich	P1918
Deposited data		
Raw and analyzed data	This study	
Experimental models: Organisms/strains		
Tg(-6.7Tru.Hcrtr2:GAL4-VP16)	[20,35]	ZFIN: ZDB-TGCONSTRCT-151028-8
Tg(UAS-E1b:Kaede)	[38]	ZFIN: ZDB-TGCONSTRCT-070314-1
Tg(-17.6isl2b:GFP)	[22]	
Tg(UAS:GCaMP6s)	[44]	ZFIN: ZDB-TGCONSTRCT-140811-3
Software and algorithms		
Fiji/ImageJ	[111]	RRID: SCR_02285
Adobe Illustrator (2021)	Adobe	RRID: SCR_010279
Matlab 2020b	Mathworks	RRID: SCR_001622

Lead Contact

Further information and requests for resources and reagents should be directed to and will be fulfilled by the lead contact, Dena Goldblatt (goldblatt.dena@gmail.com) in coordination with David Schoppik (schoppik@gmail.com).

Materials Availability

This study did not generate new unique reagents.

Data and code availability

All data and code are deposited at the Open Science Framework and are publicly available at 10.17605/OSF.IO/KP839

EXPERIMENTAL MODEL AND SUBJECT DETAILS

Fish care

All protocols and procedures involving zebrafish were approved by the New York University Langone School of Medicine Institutional Animal Care & Use Committee (IACUC). All larvae were raised at 28.5°C at a density of 20-50 larvae in 25-40 ml of buffered E3 (1mM HEPES added). Larvae used for birthdating experiments were raised in constant darkness; all other fish were raised on a standard 14/10h light/dark cycle. Larvae for experiments were between 1-5 days post-fertilization (dpf).

Transgenic lines

Experiments were conducted on the *mifta*$^{-/-}$ background to remove pigment. Validation of statoacoustic ganglion labeling by *Tg(-6.7Tru.Hcrtr2:GAL4-VP16)*[20,35] was performed using *Tg(-17.6isl2b:GFP)*. All other experiments used *Tg(-6.7Tru.Hcrtr2:GAL4-VP16)*[20,35] larvae to drive expression of the following UAS reporters: *Tg(UAS:E1b-Kaede)*[38] for birthdating only experiments and *Tg(UAS:GCaMP6s)*[112];*Tg(US:E1b-Kaede)* for acute lesion/calcium imaging experiments. Larvae used were selected for brightness of fluorescence relative to siblings. Mendelian ratios were observed, supporting that selected larvae were homozygous for a given allele.

Method details

Confocal imaging

Larvae were anesthetized in 0.2 mg/mL ethyl-3-aminobenzoic acid ethyl ester (MESAB, Sigma-Aldrich E10521, St. Louis, MO) prior to imaging except where noted. Larvae were mounted dorsal side-up (axial view) or lateral side-up (sagittal view) in 2% low-melting point agarose (Thermo Fisher Scientific 16520) in E3. Birthdating images of the vestibular ganglion were collected on a Zeiss LSM800 confocal microscope with a 20x water-immersion objective (Zeiss W Plan-Apochromat 20x/1.0). All imaging windows were 160x160µm. Anatomy stacks spanned approximately 60µm in depth (mediolateral axis), sampled every micron. For two-photon imaging of the tangential nucleus, stimulus imaging windows were 297x86µm. Anatomy stacks of the tangential nucleus spanned 50-60µm, sampled every micron (dorsoventral axis). All anatomy stacks were collected between 4-5 dpf. Raw image stacks were analyzed using Fiji/ImageJ[111].

Optical tagging of neurons by birthdate

All experiments used larvae from *Tg(-6.7Tru.Hcrtr2:GAL4-VP16);Tg(UAS:E1b-Kaede)*. Neurons were optically tagged by their time of terminal differentiation using whole-embryo Kaede photoconversions[39] as described in[26]. Briefly, embryos were photoconverted for five minutes on a custom-built apparatus with a 405 nm LED bulb. Photoconversions were performed at experimenter-defined timepoints between 22–72 hpf. Embryos used for experiments were converted at only one timepoint. Larvae were subsequently raised in darkness to prevent background photoconversion until the time of imaging (5 dpf). Neurons born before the time of conversion were identified by the presence of converted (red) Kaede. For each experiment, basal conversion was estimated by imaging control larvae raised in darkness until confocal imaging. n=5 hemispheres from N=5 separate larvae were analyzed for each timepoint. The 60 hpf timepoint was only analyzed with respect to "born after" neurons. Only one hemisphere was analyzed for each larvae.

Representations of vestibular ganglion neurons in example images and maps

The following image adjustments were performed to representative images and spatial registration data. First, to correlate the anatomy of mapped images with previous representations of vestibular ganglion topography[25], spatial maps were rotated 3.81 degrees anticlockwise. Next, the midpoints in the dorsoventral (Y) and rostrocaudal (X) axes and circumscribed boundaries shown in spatial maps and quantification plots were defined using the mean range of the n=345 neurons from N=5 *Tg(-6.7Tru.Hcrtr2:VP16-GAL4)* mapped control larvae. All representative images of photoconverted neurons ("born before") are shown after applying a threshold to subtract background and/or bleedthrough conversion (e.g., Figure 2B and Figure 5D). The thresholding method is described below ("Correction of background and/or bleedthrough Kaede conversion"). In image stacks, medial cells often appeared dimmer due to the light scattering properties of brain tissue. To aid visualization of all cells in representative maximum intensity projection images (e.g., Figure 1B, Figure 2B, and Figure 5D), brightness, contrast, and/or gamma were separately adjusted for medial and lateral planes.

Imaging and analysis of bipolar afferents

Bipolar afferent development was evaluated in the same larvae used for somatic birthdating experiments. As neuronal soma had brighter fluorescence than their bipolar afferents, to avoid oversaturation we acquired separate image stacks to evaluate projections to the VIIIth nerve and utricular macula.

Acute lesion and calcium imaging experiments

Experiments used sighted larvae from *Tg(-6.7Tru.Hcrtr2:GAL4-VP16);Tg(UAS:E1b-Kaede);Tg(UAS:GCaMP6s)*. Larvae were birthdated at 26 hpf using whole-embryo conversions, then imaged on a confocal microscope at 4 dpf to identify neurons born before photoconversion. At 5 dpf, acute, uni-lateral lesion and calcium imaging experiments were performed using a two-photon microscope. To visualize the statoacoustic ganglion, larvae were mounted lateral side-up (sagittal view). Lesions were targeted to neurons born after the time of photoconversion (green, unconverted Kaede only) in one hemisphere only. Lesions were performed using a pulsed infrared laser (SpectraPhysics Spirit 8W) at 1040 mm (400 fs pulse duration, 4 pulses per cell over 10 ms) at 25-75 nJ per pulse. Anatomy stacks of the statoacoustic ganglion were acquired before and immediately after lesions to confirm the lesion extent. Larvae were left to recover for ten minutes and re-mounted axially for calcium imaging of the tangential nucleus. Calcium imaging after pitch-tilt stimulation was performed and analyzed as described in[26,43,72]. Briefly, tonic 19°up/down tilts were delivered to larvae using a galvonometer and calcium activity was imaged immediately following tilt presentation. Control experiments used non-lesioned larvae to minimize potential off-target effects from commissural-projecting neurons.

Statistical analyses and quantification

Validation of vestibular ganglion labeling in *Tg(-6.7Tru.Hcrtr2:GAL4-VP16)*

For initial validation that *Tg(-6.7Tru.Hcrtr2:GAL4-VP16)* labels neurons within the anatomical constraints of the vestibular ganglion, *Tg(-6.7Tru.Hcrtr2:GAL4-VP16)* expression was compared directly against *Tg(-17.6isl2b:GFP)* in double transgenic embryos. *Tg(-6.7Tru.Hcrtr2:GAL4-VP16)* was labeled with a red UAS reporter (photoconverted *Tg(UAS-E1b:Kaede)*) and compared with co-localized *Tg(-17.6isl2b:GFP)* expression. After validating co-localization, all subsequent quantification of vestibular ganglion density and cell position (Figure 1D-Figure 1H) was performed in singly-labeled transgenic larvae. We evaluated n=220 neurons from N=3 *Tg(-17.6isl2b:GFP)* and n=345 neurons from N=5 *Tg(-6.7Tru.Hcrtr2:GAL4-VP16)* larvae.

Spatial registration of vestibular ganglion soma

Neurons were manually registered to a common coordinate framework in Adobe Illustrator (2021). The maximum intensity projections (MIPs) from all imaged larvae were aligned using stereotyped and clearly-identifiable anatomical landmarks: the saccule, the utricle, the edge of the otic capsule, and the VIIIth nerve branch. To control for potential bias, MIP alignment was verified by two independent observers (D.G. and S.H.). To control for differences in digital magnification across microscopes and larvae, all MIPs were uniformly scaled to a standardized resolution (5.0 pixels/µm).

Vestibular ganglion neurons labeled by *Tg(-6.7Tru.Hcrtr2:GAL4-VP16)* were approximately 10 µm in diameter. To simplify localization of neurons in the mediolateral (Z) axis, each anatomical image stack was subdivided into five, 12 µm

thick planes (Figure 1C, Figure 1E), such that each neuron would appear in no more than two mediolateral planes. Subdivisions were assessed for consistency using anatomical landmarks. The caudal-most neurons occupied the first mediolateral plane (z1), and the rostral-most neurons occupied the last mediolateral plane (z5). The mediolateral midpoint (z3) was qualitatively aligned with the dorsoventral (Y) and rostrocaudal (X) midpoints. Each mediolateral plane was aligned with its MIP. Neurons were manually localized to a mediolateral subdivision based on the plane in which the soma fluorescence was brightest (soma center). Reference neurons, represented as circles approximately the diameter of a neuron, were centered over the soma in the appropriate subdivision. The mediolateral subdivision and the rostrocaudal (X) and dorsoventral (Y) Illustrator coordinates were manually recorded for each neuron. For standardization, XY coordinates were normalized by subtraction of the upper-most and left-most coordinates. Standardized coordinates were then used to recreate a spatial map of neurons imaged across all fish in Matlab. Cell counts were concurrently performed in Fiji/ImageJ[111] using the Cell Counter plugin.

Spatial registration and quantification of converted bipolar afferent projections

Maximum intensity projections were aligned using anatomical landmarks (otic capsule, utricle, etc.) into a hyperstack in Fiji/ImageJ[111]. A 15 µm or 35 µm-sized rectangular ROI was drawn around the extent of the macula and VIIIth nerve axon projections, respectively. The fluorescence gray value along the rostrocaudal axis of the ROI was extracted using the "Plot XY Profile" function for each channel (unconverted green, converted red), and the X profile (rostrocaudal axis) was obtained. As neurons continue to generate new, unconverted Kaede fluorescence after the time of conversion, unconverted (green) fluorescence comprises projections from neurons born both before and after the time of conversion. Fluorescence values were imported into Matlab. To account for variation in Kaede fluorescence across larvae due to transgenic expression, fluorescence values were standardized by the maximum raw fluorescence observed for each fish. Probability distributions were generated, and the median/standard deviation were calculated. N=3 hemispheres/timepoint (N=1 hemisphere per larva) were quantified.

Correction of background and/or bleedthrough Kaede conversion

Basal Kaede conversion was estimated by imaging a total of N=18 unconverted (green only, sibling controls) larvae raised in darkness until imaging at 5 dpf. Control larvae had comparable fluorescence as experimental larvae and were imaged alongside experimental larvae using identical imaging settings. The amount of fluorescence observed in the red (converted Kaede) channel was measured using Fiji/ImageJ[111]. As controls were never exposed to light until the time of imaging, any red fluorescence was either basal conversion or unconverted (green) fluorescence bleedthrough. The average red Kaede fluorescence value across the vestibular ganglion was used as a "threshold" and subtracted from all birthdated images. This ensured that cells designated as born based on the presence of red Kaede were not artifacts of basal or bleedthrough fluorescence.

Statistical analysis of spatial organization

For each timepoint, data from all hemispheres analyzed (N=5/timepoint) were pooled given variability in the number of vestibular ganglion neurons labeled across transgenic larve (median: 77±15 neurons/fish across N=5 control hemispheres; see Figure 1H). The number of "born before" and "born after" neurons mapped per fish is listed in Table 1. Probability distributions of soma position were generated using the median and standard deviation from pooled and bootstrapped data (n=100 iterations). Spatial organization was evaluated individually in each spatial axis using a two-tailed Kolmogorov-Smirnov (KS) test given that most distributions were bimodal. All control distributions used the n=345 neurons mapped from the N=5 *Tg(-6.7Tru.Hcrtr2:GAL4-VP16)* control larvae described above.

Quantification and analysis of acute lesion and calcium imaging experiments

Calcium responses in the tangential nucleus were extracted and analyzed as described in[26,72]. In Fiji/ImageJ, regions of interest (ROI) were drawn around each tangential nucleus soma and raw fluorescence values were extracted using Matlab. Calcium responses were normalized using the mean fluorescence value of a baseline period, and the first second of the calcium response was used for analysis. Responses were analyzed with respect to two primary metrics: (1) nose-up/nose-down identity, defined using a directionality index that compared the calcium responses to up/down tilt stimulation; (2) spatial organization, mapped in Illustrator using the same methodology as described above and in[26,72].f In cell position maps, plotted neuron centers were scaled to match the strength of their fluorescence responses, evaluated using the maximum value of the $\Delta F/F$ fluorescent response.

All identifiable neurons within the tangential nucleus were analyzed. We analyzed the responses of n=140 tangential nucleus neurons from N=4 control, never-lesioned larvae (median: 36±7 neurons/larva) and n=110 neurons from N=4 larvae following acute, uni-lateral vestibular ganglion lesion (median: 28±5 neurons/larva). Qualitatively, we observed that tangential nucleus neurons in larvae after vestibular ganglion lesions had lower basal fluorescence, which may account for variation in the number of identifiable neurons per larva. All Wilcoxon rank sum tests for differences of medians were performed on a per-larva basis. Statistical analysis of neuron position were performed on aggregate data from all larvae to account for spatial biases in transgenic expression.

ACKNOWLEDGMENTS

Research was supported by the National Institute on Deafness and Communication Disorders of the National Institutes of Health under award numbers R01DC017489 and the National Institute of Neurological Disorders and Stroke under award numbers F99NS129179, T32NS086750. The authors would like to thank Hannah Gelnaw for assistance with fish care, and Jeremy Dasen, Claude Desplan, Katherine Nagel, and Dan Sanes, along with the members of the Schoppik and Nagel labs for their valuable feedback and discussions.

AUTHOR CONTRIBUTIONS

Conceptualization: SH, DG and DS, Methodology: SH, DG and DS, Investigation: SH, MRG, and SND, Visualization: SH, Writing: SH, Editing: DG and DS, Funding Acquisition: DG and DS, Supervision: DG.

AUTHOR COMPETING INTERESTS

The authors declare no competing interests.

REFERENCES

1. Gülşen Sürmeli, Turgay Akay, Gregory C. Ippolito, Philip W. Tucker, and Thomas M. Jessell. Patterns of spinal sensory-motor connectivity prescribed by a dorsoventral positional template. *Cell*, 147(3):653–665, October 2011.
2. Nikolaos Balaskas, David Ng, and Niccolò Zampieri. The positional logic of sensory-motor reflex circuit assembly. *Neuroscience*, 450:142150, December 2020.
3. Eric I. Knudsen and Michael S. Brainard. Visual instruction of the neural map of auditory space in the developing optic tectum. *Science*, 253(5015):85–87, July 1991.
4. Jianhua Cang and David A. Feldheim. Developmental mechanisms of topographic map formation and alignment. *Annual Review of Neuroscience*, 36(1):5177, July 2013.
5. Jay B. Bikoff, Mariano I. Gabitto, Andre F. Rivard, Estelle Drobac, Timothy A. Machado, Andrew Miri, Susan Brenner-Morton, Erica Famojure, Carolyn Diaz, Francisco J. Alvarez, George Z. Mentis, and Thomas M. Jessell. Spinal inhibitory interneuron diversity delineates variant motor microcircuits. *Cell*, 165(1):207–219, mar 2016.
6. Wilder Penfield and Edwin Boldrey. Somatic motor and sensory representation in the cereberal cortex of man as studied by electrical stimulation. *Brain*, 60(4):389–443, 1937.
7. Reha S. Erzurumlu, Yasunori Murakami, and Filippo M. Rijli. Mapping the face in the somatosensory brainstem. *Nature Reviews Neuroscience*, 11(4):252–263, February 2010.
8. Ariel J Levine, Kathryn A Lewallen, and Samuel L Pfaff. Spatial organization of cortical and spinal neurons controlling motor behavior. *Current Opinion in Neurobiology*, 22(5):812–821, October 2012.
9. Isabel Holguera and Claude Desplan. Neuronal specification in space and time. *Science*, 362(6411):176180, October 2018.
10. Aisha Hamid, Hannah Gattuso, Aysu Nora Caglar, Midhula Pillai, Theresa Steele, Alexa Gonzalez, Katherine Nagel, and Mubarak Hussain Syed. The conserved rna-binding protein imp is required for the specification and function of olfactory navigation circuitry in drosophila. *Current Biology*, 34(3):473–488.e6, February 2024.
11. Brandon Mark, Sen-Lin Lai, Aref Arzan Zarin, Laurina Manning, Heather Q Pollington, Ashok Litwin-Kumar, Albert Cardona, James W Truman, and Chris Q Doe. A developmental framework linking neurogenesis and circuit formation in the drosophila CNS. *eLife*, 10, May 2021.
12. Austin Q. Seroka and Chris Q. Doe. The hunchback temporal transcription factor determines motor neuron axon and dendrite targeting in *Drosophila*. *Development*, January 2019.
13. Christopher C. Wreden, Julia L. Meng, Weidong Feng, Wanhao Chi, Zarion D. Marshall, and Ellie S. Heckscher. Temporal cohorts of lineage-related neurons perform analogous functions in distinct sensorimotor circuits. *Current Biology*, 27(10):1521–1528.e4, May 2017.
14. Julia L Meng, Zarion D Marshall, Meike Lobb-Rabe, and Ellie S Heckscher. How prolonged expression of hunchback, a temporal transcription factor, re-wires locomotor circuits. *eLife*, 8, September 2019.
15. Avinash Pujala and Minoru Koyama. Chronology-based architecture of descending circuits that underlie the development of locomotor repertoire after birth. *eLife*, 8, February 2019.
16. D. L. McLean and J. R. Fetcho. Spinal interneurons differentiate sequentially from those driving the fastest swimming movements in larval zebrafish to those driving the slowest ones. *Journal of Neuroscience*, 29(43):13566–13577, October 2009.
17. Joseph R. Fetcho and David L. McLean. Some principles of organization of spinal neurons underlying locomotion in zebrafish and their implications. *Annals of the New York Academy of Sciences*, 1198(1):94–104, Jun 2010.
18. Sandeep Kishore, Eli B. Cadoff, Moneeza A. Agha, and David L. McLean. Orderly compartmental mapping of premotor inhibition in the developing zebrafish spinal cord. *Science*, 370(6515):431–436, October 2020.
19. J. Szentágothai. Pathways and synaptic articulation patterns connecting vestibular receptors and oculomotor nuclei. In *The Oculomotor System*, pages 205–223. Hoeber Medical Division, Harper and Row, 1964.
20. David Schoppik, Isaac H. Bianco, David A. Prober, Adam D. Douglass, Drew N. Robson, Jennifer M.B. Li, Joel S.F. Greenwood, Edward Soucy, Florian Engert, and Alexander F. Schier. Gaze-stabilizing central vestibular neurons project asymmetrically to extraocular motoneuron pools. *The Journal of Neuroscience*, 37(47):11353–11365, sep 2017.
21. S. Higashijima, Y. Hotta, and H. Okamoto. Visualization of cranial motor neurons in live transgenic zebrafish expressing green fluorescent protein under the control of the *Islet*-1 promoter/enhancer. *Journal of Neuroscience*, 20(1):206–218, Jan 2000.
22. A. J. Pittman, M.-Y. Law, and C.-B. Chien. Pathfinding in a large vertebrate axon tract: isotypic interactions guide retinotectal axons at multiple choice points. *Development*, 135(17):2865–2871, sep 2008.
23. Martha W Bagnall and David Schoppik. Development of vestibular behaviors in zebrafish. *Current Opinion in Neurobiology*, 53:83–89, December 2018.
24. Masashi Tanimoto, Ikuko Watakabe, and Shin ichi Higashijima. Tiltable objective microscope visualizes discrimination of static and dynamic head movement originates at hair cells. *bioRxiv*, July 2022.
25. Zhikai Liu, David G. C. Hildebrand, Joshua L. Morgan, Yizhen Jia, Nicholas Slimmon, and Martha W. Bagnall. Organization of the gravity-sensing system in zebrafish. *Nature Communications*, 13(1), August 2022.
26. Dena Goldblatt, Stephanie Huang, Marie R. Greaney, Kyla R. Hamling, Venkatakaushik Voleti, Citlali Perez-Campos, Kripa B. Patel, Wenze Li, Elizabeth M.C. Hillman, Martha W. Bagnall, and David Schoppik. Neuronal birthdate reveals topography in a vestibular brainstem circuit for gaze stabilization. *Current Biology*, 33(7):1265–1281.e7, April 2023.
27. Marie R. Greaney, Ann E. Privorotskiy, Kristen P. D'Elia, and David Schoppik. Extraocular motoneuron pools develop along a dorsoventral axis in zebrafish, *Danio rerio*. *Journal of Comparative Neurology*, 525(1):65–78, jun 2016.
28. Shruti Vemaraju, Husniye Kantarci, Mahesh S. Padanad, and Bruce B. Riley. A spatial and temporal gradient of fgf differentially regulates distinct stages of neural development in the zebrafish inner ear. *PLoS Genetics*, 8(11):e1003068, November 2012.
29. Dora Sapède and Cristina Pujades. Hedgehog signaling governs the development of otic sensory epithelium and its associated innervation in zebrafish. *The Journal of Neuroscience*, 30(10):36123623, March 2010.
30. Laura Taberner, Aitor Bañón, and Berta Alsina. Anatomical map of the cranial vasculature and sensory ganglia. *Journal of Anatomy*, 232(3):431439, December 2017.

31. Dora Sapède, Sylvia Dyballa, and Cristina Pujades. Cell lineage analysis reveals three different progenitor pools for neurosensory elements in the otic vesicle. *The Journal of Neuroscience*, 32(46):1642416434, November 2012.
32. A. Zecca, S. Dyballa, A. Voltes, R. Bradley, and C. Pujades. The order and place of neuronal differentiation establish the topography of sensory projections and the entry points within the hindbrain. *Journal of Neuroscience*, 35(19):7475–7486, may 2015.
33. Sylvia Dyballa, Thierry Savy, Philipp Germann, Karol Mikula, Mariana Remesikova, Róbert Špir, Andrea Zecca, Nadine Peyriéras, and Cristina Pujades. Distribution of neurosensory progenitor pools during inner ear morphogenesis unveiled by cell lineage reconstruction. *eLife*, 6, jan 2017.
34. Richard Roberts, Jeffrey Elsner, and Martha W. Bagnall. Delayed otolith development does not impair vestibular circuit formation in zebrafish. *Journal of the Association for Research in Otolaryngology*, 18(3):415–425, March 2017.
35. Alix M.B. Lacoste, David Schoppik, Drew N. Robson, Martin Haesemeyer, Ruben Portugues, Jennifer M. Li, Owen Randlett, Caroline L. Wee, Florian Engert, and Alexander F. Schier. A convergent and essential interneuron pathway for mauthner-cell-mediated escapes. *Current Biology*, 25(11):1526–1534, jun 2015.
36. Isaac H. Bianco, Leung-Hang Ma, David Schoppik, Drew N. Robson, Michael B. Orger, James C. Beck, Jennifer M. Li, Alexander F. Schier, Florian Engert, and Robert Baker. The tangential nucleus controls a gravito-inertial vestibulo-ocular reflex. *Current Biology*, 22(14):1285–1295, Jul 2012.
37. Paige Leary, Celine Bellegarda, Cheryl Quainoo, Dena Goldblatt, Basak Rosti, and David Schoppik. Sensation is dispensable for the maturation of the vestibulo-ocular reflex. *bioRxiv*, May 2024.
38. Ethan K. Scott, Lindsay Mason, Aristides B. Arrenberg, Limor Ziv, Nathan J Gosse, Tong Xiao, Neil C. Chi, Kazuhide Asakawa, Koichi Kawakami, and Herwig Baier. Targeting neural circuitry in zebrafish using GAL4 enhancer trapping. *Nature Methods*, mar 2007.
39. S. J. C. Caron, D. Prober, M. Choy, and A. F. Schier. *In vivo* birthdating by BAPTISM reveals that trigeminal sensory neuron diversity depends on early neurogenesis. *Development*, 135(19):3259–3269, Aug 2008.
40. Catherine Haddon and Julian Lewis. Early ear development in the embryo of the zebrafish, danio rerio. *The Journal of Comparative Neurology*, 365(1):113128, January 1996.
41. Jeremy S. Dasen. *Chapter 4 Transcriptional Networks in the Early Development of SensoryMotor Circuits*, page 119148. Elsevier, 2009.
42. Gulen Surmeli, Turgay Akay, GregoryăC. Ippolito, PhilipăW. Tucker, and ThomasăM. Jessell. Patterns of spinal sensory-motor connectivity prescribed by a dorsoventral positional template. *Cell*, 147(3):653665, October 2011.
43. Kyla R. Hamling, Yunlu Zhu, Franziska Auer, and David Schoppik. Tilt in place microscopy: a simple, low-cost solution to image neural responses to body rotations. *The Journal of Neuroscience*, 43(6):936948, December 2022.
44. Tsai-Wen Chen, Trevor J. Wardill, Yi Sun, Stefan R. Pulver, Sabine L. Renninger, Amy Baohan, Eric R. Schreiter, Rex A. Kerr, Michael B. Orger, Vivek Jayaraman, Loren L. Looger, Karel Svoboda, and Douglas S. Kim. Ultrasensitive fluorescent proteins for imaging neuronal activity. *Nature*, 499(7458):295–300, July 2013.
45. E. J. Koundakjian, J. L. Appler, and L. V. Goodrich. Auditory neurons make stereotyped wiring decisions before maturation of their targets. *Journal of Neuroscience*, 27(51):14078–14088, December 2007.
46. Donald Bell, Andrea Streit, Itziar Gorospe, Isabel Varela-Nieto, Berta Alsina, and Fernando Giraldez. Spatial and temporal segregation of auditory and vestibular neurons in the otic placode. *Developmental Biology*, 322(1):109120, October 2008.
47. Aitor Bañón and Berta Alsina. Pioneer statoacoustic neurons guide neuroblast behaviour during otic ganglion assembly. *Development*, 150(21), November 2023.
48. Surjit Singh Saini and Raj K. Ladher. Timing of delamination of inner ear neurons specifies their topography and target innervation. *bioRxiv*, November 2024.
49. Alejandra S. Laureano, Kathleen Flaherty, Anna-Maria Hinman, Azadeh Jadali, Tetsuya Nakamura, Shin-ichi Higashijima, Hatim E. Sabaawy, and Kelvin Y. Kwan. shox2 is required for vestibular statoacoustic neuron development. *Biology Open*, 11(12), December 2022.
50. Katherine L. Hammond and Tanya T. Whitfield. Fgf and hh signalling act on a symmetrical pre-pattern to specify anterior and posterior identity in the zebrafish otic placode and vesicle. *Development*, 138(18):39773987, September 2011.
51. Esther C. Maier and Tanya T. Whitfield. Ra and fgf signalling are required in the zebrafish otic vesicle to pattern and maintain ventral otic identities. *PLoS Genetics*, 10(12):e1004858, December 2014.
52. Tanya T. Whitfield, Bruce B. Riley, MingYung Chiang, and Bryan Phillips. Development of the zebrafish inner ear. *Developmental Dynamics*, 223(4):427458, March 2002.
53. Catherine Haddon, Yun-Jin Jiang, Lucy Smithers, and Julian Lewis. Delta-notch signalling and the patterning of sensory cell differentiation in the zebrafish ear: evidence from the mind bomb mutant. *Development*, 125(23):46374644, December 1998.
54. Charles B. Kimmel, Kohei Hatta, and Walter K. Metcalfe. Early axonal contacts during development of an identified dendrite in the brain of the zebrafish. *Neuron*, 4(4):535545, April 1990.
55. J. Pujol-Marti, A. Zecca, J.-P. Baudoin, A. Faucherre, K. Asakawa, K. Kawakami, and H. Lopez-Schier. Neuronal birth order identifies a dimorphic sensorineural map. *Journal of Neuroscience*, 32(9):2976–2987, February 2012.
56. Simone Schwarzer, Nandini Asokan, Oliver Bludau, Jeongeun Chae, Veronika Kuscha, Jan Kaslin, and Stefan Hans. Neurogenesis in the inner ear: the zebrafish statoacoustic ganglion provides new neurons from a neurod/nestin-positive progenitor pool well into adulthood. *Development*, 147(7), April 2020.
57. Sedigheh Delmaghani and Aziz El-Amraoui. The genetic and phenotypic landscapes of usher syndrome: from disease mechanisms to a new classification. *Human Genetics*, 141(34):709735, March 2022.
58. Takumi Sugioka, Masashi Tanimoto, and Shin-ichi Higashijima. Biomechanics and neural circuits for vestibular-induced fine postural control in larval zebrafish. *Nature Communications*, 14(1), March 2023.
59. Joseph Altman and Shirley A. Bayer. Development of the brain stem in the rat. V. Thymidine-radiographic study of the time of origin of neurons in the midbrain tegmentum. *The Journal of Comparative Neurology*, 198(4):677–716, Jun 1981.
60. Joel C. Glover. The development of vestibulo-ocular circuitry in the chicken embryo. *Journal of Physiology-Paris*, 97(1):17–25, Jan 2003.
61. Adel Maklad and Bernd Fritzsch. Development of vestibular afferent projections into the hindbrain and their central targets. *Brain Research Bulletin*, 60(56):497510, June 2003.
62. Franois Auclair, Raymond Marchand, and Joel C. Glover. Regional patterning of reticulospinal and vestibulospinal neurons in the hindbrain of mouse and rat embryos. *The Journal of Comparative Neurology*, 411(2):288300, August 1999.
63. Marjorie D. Shaw and Keith E. Alley. Generation of the ocular motor nuclei and their cell types in the rabbit. *The Journal of Comparative Neurology*, 200(1):69–82, Jul 1981.
64. Luis Puelles and Alain Privat. Do oculomotor neuroblasts migrate across the midline in the fetal rat brain? *Anatomy and Embryology*, 150(2):187206, 1977.
65. JOEL C. GLOVER. Development of secondorder vestibular projections in the chicken embryoa. *Annals of the New York Academy of Sciences*, 781(1):1320, June 1996.
66. Masashi Tanimoto, Yukiko Ota, Kazuki Horikawa, and Yoichi Oda. Auditory input to cns is acquired coincidentally with development of inner ear after formation of functional afferent pathway in zebrafish. *The Journal of Neuroscience*, 29(9):27622767, March 2009.
67. Masashi Tanimoto, Yukiko Ota, Maya Inoue, and Yoichi Oda. Origin of inner ear hair cells: Morphological and functional differentiation from ciliary cells into hair cells in zebrafish inner ear. *The Journal of Neuroscience*, 31(10):37843794, March 2011.
68. Bruce B. Riley, Chenwei Zhu, Chris Janetopoulos, and Karl J. Aufderheide. A critical period of ear development controlled by distinct populations of ciliated cells in the zebrafish. *Developmental Biology*, 191(2):191201, November 1997.
69. B. Fritzsch and D.H. Nichols. Dii reveals a prenatal arrival of efferents at the differentiating otocyst of mice. *Hearing Research*, 65(12):5160, February 1993.
70. Joseph Altman and Shirley A. Bayer. *Development of the Cranial Nerve Ganglia and Related Nuclei in the Rat*. Springer Berlin Heidelberg, 1982.
71. C. Clark, O. Austen, I. Poparic, and S. Guthrie. α2-chimaerin regulates a key axon guidance transition during development of the oculomotor projection. *Journal of Neuroscience*, 33(42):16540–16551, Oct 2013.
72. Dena Goldblatt, Baak Rosti, Kyla R. Hamling, Paige Leary, Harsh Panchal, Marlyn Li, Hannah Gelnaw, Stephanie Huang, Cheryl Quainoo, and David Schoppik. Motor neurons are dispensable for the assembly of a sensorimotor circuit for gaze stabilization. *eLife*, April 2024.
73. P Wenner and E Frank. Peripheral target specification of synaptic connectivity of muscle spindle sensory neurons with spinal motoneurons. *The Journal of Neuroscience*, 15(12):81918198, December 1995.

74. Sebastian Poliak, Amy L. Norovich, Masahito Yamagata, Joshua R. Sanes, and Thomas M. Jessell. Muscle-type identity of proprioceptors specified by spatially restricted signals from limb mesenchyme. *Cell*, 164(3):512525, January 2016.
75. Silvia Arber. Motor circuits in action: Specification, connectivity, and function. *Neuron*, 74(6):975–989, jun 2012.
76. Dawei Wu, Ira Schieren, Yingzhi Qian, Chaolin Zhang, Thomas M. Jessell, and Joriene C. de Nooij. A role for sensory end organ-derived signals in regulating muscle spindle proprioceptor phenotype. *The Journal of Neuroscience*, 39(22):42524267, March 2019.
77. Amy L. Norovich, Susan Brenner-Morton, and Thomas M. Jessell. Muscle-derived cues are required to specify proprioceptor pool identity. *bioRxiv*, August 2022.
78. Florian Ulrich, Charlotte Grove, Jesús Torres-Vázquez, and Robert Baker. Development of functional hindbrain oculomotor circuitry independent of both vascularization and neuronal activity in larval zebrafish. *Current Neurobiology*, 7:62–73, 2014.
79. David H. Hubel and Torsten N. Wiesel. Effects of monocular deprivation in kittens. *Naunyn-Schmiedebergs Archiv fr Experimentelle Pathologie und Pharmakologie*, 248(6):492497, 1964.
80. J.T. Schmidt and L.E. Eisele. Stroboscopic illumination and dark rearing block the sharpening of the regenerated retinotectal map in goldfish. *Neuroscience*, 14(2):535546, February 1985.
81. Joshua R. Sanes and S. Lawrence Zipursky. Synaptic specificity, recognition molecules, and assembly of neural circuits. *Cell*, 181(3):536556, April 2020.
82. Olivia Spead, Trevor Moreland, Cory J. Weaver, Irene Dalla Costa, Brianna Hegarty, Kenneth L. Kramer, and Fabienne E. Poulain. Teneurin trans-axonal signaling prunes topographically missorted axons. *Cell Reports*, 42(3):112192, March 2023.
83. M. Berry, A. W. Rogers, and J. T. Eayrs. Pattern of cell migration during cortical histogenesis. *Nature*, 203(4945):591–593, August 1964.
84. Omer Ali Bayraktar and Chris Q. Doe. Combinatorial temporal patterning in progenitors expands neural diversity. *Nature*, 498(7455):449–455, June 2013.
85. Xin Li, Ted Erclik, Claire Bertet, Zhenqing Chen, Roumen Voutev, Srinidhi Venkatesh, Javier Morante, Arzu Celik, and Claude Desplan. Temporal patterning of drosophila medulla neuroblasts controls neural fates. *Nature*, 498(7455):456–462, June 2013.
86. Lori Glenwinkel, Seth R Taylor, Kasper Langebeck-Jensen, Laura Pereira, Molly B Reilly, Manasa Basavaraju, Ibnul Rafi, Eviatar Yemini, Roger Pocock, Nenad Sestan, Marc Hammarlund, David M Miller, and Oliver Hobert. In silico analysis of the transcriptional regulatory logic of neuronal identity specification throughout the c. elegans nervous system. *eLife*, 10, June 2021.
87. Luis F Sullivan, Timothy L Warren, and Chris Q Doe. Temporal identity establishes columnar neuron morphology, connectivity, and function in a drosophila navigation circuit. *eLife*, 8, February 2019.
88. Julia L Meng, Yupu Wang, Robert A Carrillo, and Ellie S Heckscher. Temporal transcription factors determine circuit membership by permanently altering motor neuron-to-muscle synaptic partnerships. *eLife*, 9, May 2020.
89. Stephanie Fore, Francisca Acuña-Hinrichsen, Kadir Aytac Mutlu, Ewelina Magdalena Bartoszek, Bram Serneels, Nicholas Guy Faturos, Khac Thanh Phong Chau, Mehmet Ilyas Cosacak, Carmen Diaz Verdugo, Fabrizio Palumbo, Christa Ringers, Nathalie Jurisch-Yaksi, Caghan Kizil, and Emre Yaksi. Functional properties of habenular neurons are determined by developmental stage and sequential neurogenesis. *Science Advances*, 6(36), September 2020.
90. Roman Huszár, Yunchang Zhang, Heike Blockus, and György Buzsáki. Preconfigured dynamics in the hippocampus are guided by embryonic birthdate and rate of neurogenesis. *Nature Neuroscience*, August 2022.
91. Maroun Abi Younes, Mohamad Rima, Jean-Pierre Coutanceau, Ninon Peysson, Fatemeh Hoseinkhani, Edson Rodrigues, Erika Bullier, Pascal Legendre, Jean-Marie Mangin, and Elim Hong. Birth order specified recruitment of motor circuits during spontaneous neural activity in zebrafish embryo. *bioRxiv*, August 2024.
92. David L. McLean, Jingyi Fan, Shin ichi Higashijima, Melina E. Hale, and Joseph R. Fetcho. A topographic map of recruitment in spinal cord. *Nature*, 446(7131):71–75, March 2007.
93. Gabrielle R. Barsh, Adam J. Isabella, and Cecilia B. Moens. Vagus motor neuron topographic map determined by parallel mechanisms of hox5 expression and time of axon initiation. *Current Biology*, 27(24):3812–3825.e3, December 2017.
94. Adam J. Isabella, Jason A. Stonick, Julien Dubrulle, and Cecilia B. Moens. Intrinsic positional memory guides target-specific axon regeneration in the zebrafish vagus nerve. *Development*, 148(18), September 2021.
95. Jianhua Cang, Cristopher M. Niell, Xiaorong Liu, Cory Pfeiffenberger, David A. Feldheim, and Michael P. Stryker. Selective disruption of one cartesian axis of cortical maps and receptive fields by deficiency inăephrin-as and structured activity. *Neuron*, 57(4):511523, February 2008.
96. R. W. Sperry. Chemoaffinity in the orderly growth of never fiber patterns and connections. *Proceedings of the National Academy of Sciences*, 50(4):703–710, October 1963.
97. Hwai-Jong Cheng, Masaru Nakamoto, Andrew D Bergemann, and John G Flanagan. Complementary gradients in expression and binding of elf-1 and mek4 in development of the topographic retinotectal projection map. *Cell*, 82(3):371381, August 1995.
98. John G. Flanagan and Pierre Vanderhaeghen. The ephrins and eph receptors in neural development. *Annual Review of Neuroscience*, 21(1):309345, March 1998.
99. Jason W. Triplett and David A. Feldheim. Eph and ephrin signaling in the formation of topographic maps. *Seminars in Cell & Developmental Biology*, 23(1):715, February 2012.
100. Mark Dombrovski, Yixin Zang, Giovanni Frighetto, Andrea Vaccari, Hyojong Jang, Parmis S. Mirshahidi, Fangming Xie, Piero Sanfilippo, Bryce W. Hina, Aadil Rehan, Roni H. Hussein, Pegah S. Mirshahidi, Catherine Lee, Mark A. Frye, Catherine R. von Reyn, Yerbol Z. Kurmangaliyev, Gwyneth M. Card, and S. Lawrence Zipursky. Gradients of recognition molecules shape synaptic specificity of a visuomotor transformation. *bioRxiv*, September 2024.
101. Milan Petrovic and Thomas Hummel. Temporal identity in axonal target layer recognition. *Nature*, 456(7223):800803, November 2008.
102. Shaul Yogev and Kang Shen. Cellular and molecular mechanisms of synaptic specificity. *Annual Review of Cell and Developmental Biology*, 30(1):417437, October 2014.
103. Gregory S. X. E. Jefferis, Elizabeth C. Marin, Reinhard F. Stocker, and Liqun Luo. Target neuron prespecification in the olfactory map of drosophila. *Nature*, 414(6860):204–208, November 2001.
104. Christopher L. Rees, Keivan Moradi, and Giorgio A. Ascoli. Weighing the evidence in peters rule: Does neuronal morphology predict connectivity? *Trends in Neurosciences*, 40(2):6371, February 2017.
105. Isabel Zhang, Giulia LM Boezio, Jake Cornwall-Scoones, Thomas Frith, Ming Jiang, Michael Howell, Robin Lovell-Badge, Andreas Sagner, James Briscoe, and M Joaquina Delás. The cis-regulatory logic integrating spatial and temporal patterning in the vertebrate neural tube. *bioRxiv*, April 2024.
106. WilliamăJ. Joo, LoraăB. Sweeney, Liang Liang, and Liqun Luo. Linking cell fate, trajectory choice, and target selection: Genetic analysis of sema-2b in olfactory axon targeting. *Neuron*, 78(4):673686, May 2013.
107. Yerbol Z Kurmangaliyev, Juyoun Yoo, Samuel A LoCascio, and S Lawrence Zipursky. Modular transcriptional programs separately define axon and dendrite connectivity. *eLife*, 8, November 2019.
108. Maggie M Shin, Catarina Catela, and Jeremy Dasen. Intrinsic control of neuronal diversity and synaptic specificity in a proprioceptive circuit. *eLife*, 9, August 2020.
109. Andreas Sagner, Isabel Zhang, Thomas Watson, Jorge Lazaro, Manuela Melchionda, and James Briscoe. A shared transcriptional code orchestrates temporal patterning of the central nervous system. *PLOS Biology*, 19(11):e3001450, November 2021.
110. Anders Lunde, Benjamin W. Okaty, Susan M. Dymecki, and Joel C. Glover. Molecular profiling defines evolutionarily conserved transcription factor signatures of major vestibulospinal neuron groups. *eneuro*, 6(1):ENEURO.0475–18.2019, January 2019.
111. Johannes Schindelin, Ignacio Arganda-Carreras, Erwin Frise, Verena Kaynig, Mark Longair, Tobias Pietzsch, Stephan Preibisch, Curtis Rueden, Stephan Saalfeld, Benjamin Schmid, Jean-Yves Tinevez, Daniel James White, Volker Hartenstein, Kevin Eliceiri, Pavel Tomancak, and Albert Cardona. Fiji: an open-source platform for biological-image analysis. *Nature Methods*, 9(7):676–682, Jun 2012.
112. Tod R. Thiele, Joseph C. Donovan, and Herwig Baier. Descending control of swim posture by a midbrain nucleus in zebrafish. *Neuron*, 83(3):679–691, August 2014.

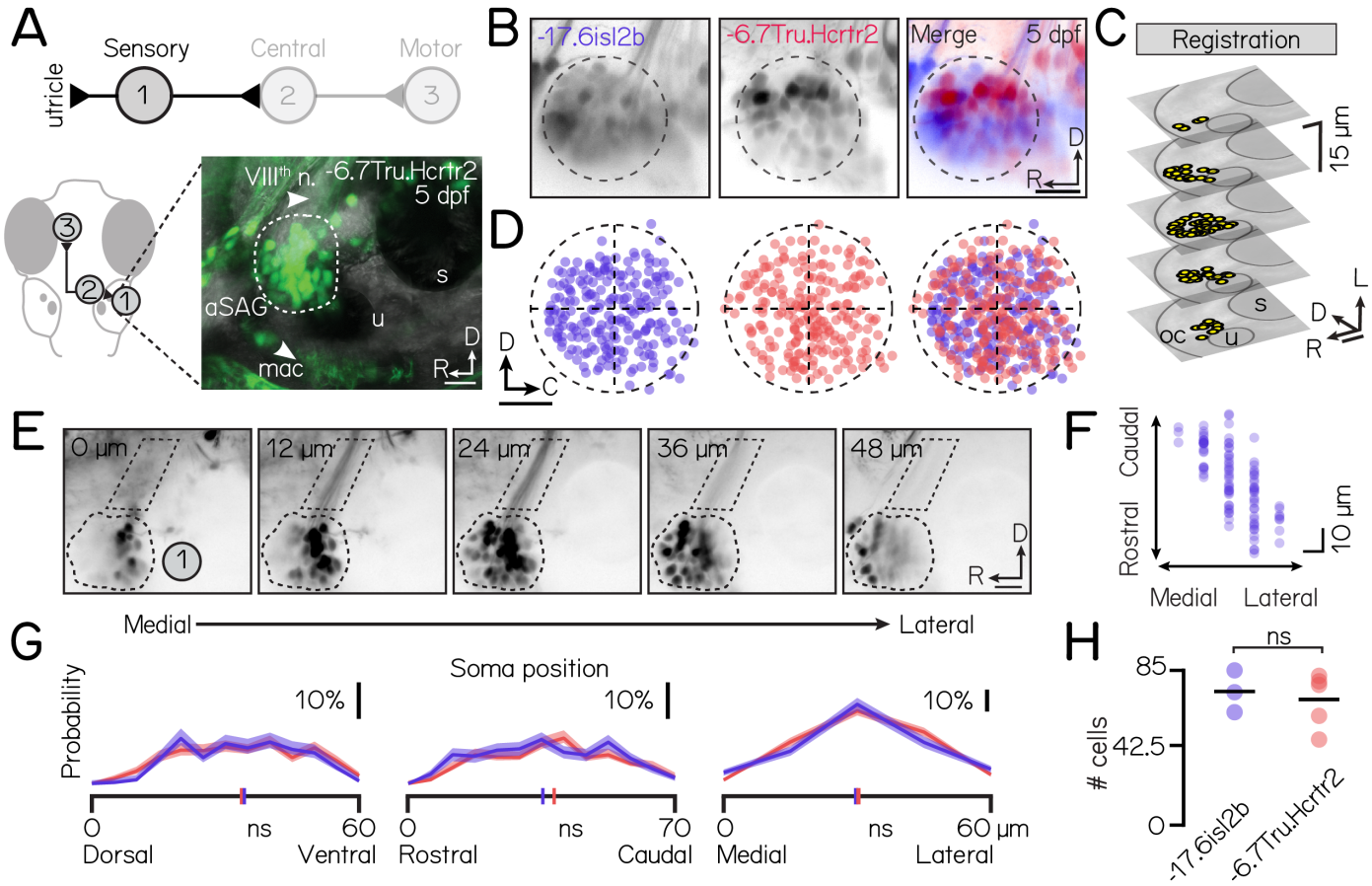

Figure 1: *Tg(-6.7Tru.Hcrtr2:GAL4-VP16)* and *Tg(-17.6isl2b:GFP)* provide comparable genetic access to vestibular sensory neurons in the anterior statoacoustic ganglion.

(A) Schematic of information flow in the vestibulo-ocular reflex circuit. Bipolar sensory neurons in the vestibular (anterior) ganglion are highlighted as the population of focus. Inset shows transmitted light image of the vestibular ganglion, labeled in green by *Tg(-6.7Tru.Hcrtr2:GAL4-VP16);Tg(UAS-E1b:Kaede)*. White arrows point to bipolar afferents to the utricular macula (bottom) and VIIIth nerve (top). mac, utricular macula; u, utricle; s, saccule; aSAG, anterior statoacoustic ganglion.

(B) Comparison of vestibular ganglion neurons labeled by *Tg(-17.6isl2b:GFP)* (left; cyan) and *Tg(-6.7Tru.Hcrtr2:GAL4-VP16);Tg(UAS-E1b:Kaede)* (middle; red) in the same larva. White dashed circle outlines the extent of the vestibular ganglion.

(C) Schematic of neuron registration method using anatomical landmarks: otic capsule (oc), utricule (u), and saccule (s).

(D) Soma position of mapped neurons labeled by *Tg(-17.6isl2b:GFP)* (n=220 neurons from N=3 larvae) or *Tg(-6.7Tru.Hcrtr2:GAL4-VP16);Tg(UAS-E1b:Kaede)* (n=345 neurons from n=5 larvae; n=220 neurons shown). Vertical and horizontal dashed lines show the rostrocaudal and dorsoventral midpoints based on the full extent of *Tg(-6.7Tru.Hcrtr2:VP16-GAL4)* expression (Methods).

(E) Representative images of the vestibular ganglion across five mediolateral subdivisions, as schematized in Figure 1C. Black dashed lines outline ganglion soma (circle) and axon projections along the VIIIth nerve (rectangle).

(F) Soma position of the n=345 mapped neurons from *Tg(-6.7Tru.Hcrtr2:GAL4-VP16)* in the orthogonal axis (mediolateral) to Figure 1D.

(G) Probability of soma position in each spatial axis for all neurons mapped in Figure 1D. Solid and shaded lines shown the mean and standard deviation, respectively using bootstrapped estimates of variance (Methods). Short vertical lines indicate the median position of all mapped neurons. n.s., not significant.

(H) Number of neurons counted in each transgenic line. Each circle is an individual fish. Data from same larvae mapped in Figure 1D. Solid bar shows mean across larvae.

All scale bars, 20µm.

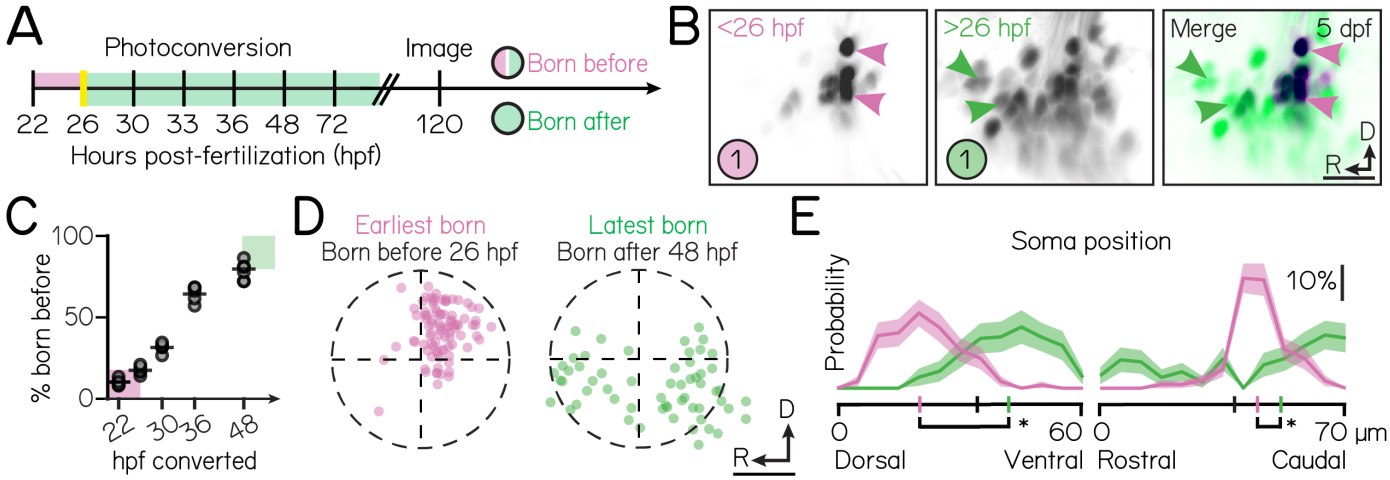

Figure 2: Early- and late-born cohorts of vestibular ganglion neurons are dorsoventrally opposed.
(A) Timeline of birthdating and imaging experiments. Time of differentiation is estimated by the presence of red, converted Kaede (born before the time of photoconversion) or green, unconverted Kaede only (born after photoconversion). Timeline shows all experimenter-defined conversion points; each larvae is converted only once. Yellow line highlights 26 hpf as the example timepoint shown in Figure 2B.
(B) Example neurons born before (left; magenta arrows) or after (middle; green arrows) 26 hpf (right: merge). Neurons are visualized by *Tg(-6.7Tru.Hcrtr2:GAL4-VP16);Tg(UAS-E1b:Kaede)* and imaged at 5 dpf. The "born before 26 hpf" image shown was thresholded to subtract background fluorescence (Methods).
(C) Percent of neurons in each fish that were born before each timepoint. Black lines indicate the mean number across individual fish (circles). N=5 fish for each age. Magenta and green shaded bars highlight the number of neurons born at the timepoints selected in Figure 2D.
(D) Location of neurons born before 26 hpf (left; "earliest-born" cohort) or after 48 hpf (right; "latest-born" cohort). Number of mapped neurons: early, n=88 neurons from N=10 fish (22 hpf and 26 hpf timepoints combined); late, n=58 neurons from N=5 fish. Dashed horizontal and vertical reference lines indicate the rostrocaudal and dorsoventral midpoints of the control neurons shown in Figure 1D.
(E) Probability of soma position for the neurons shown in Figure 2D. Short vertical axis lines indicate the median position for control (black), early-born (magenta), or late-born (green) neurons. Solid and shaded lines shown the mean and standard deviation, respectively using bootstrapped estimates of variance (Methods).
All scale bars, 20µm. Stars denote significance at the $p<0.05$ level; full statistics are shown in Table 2.

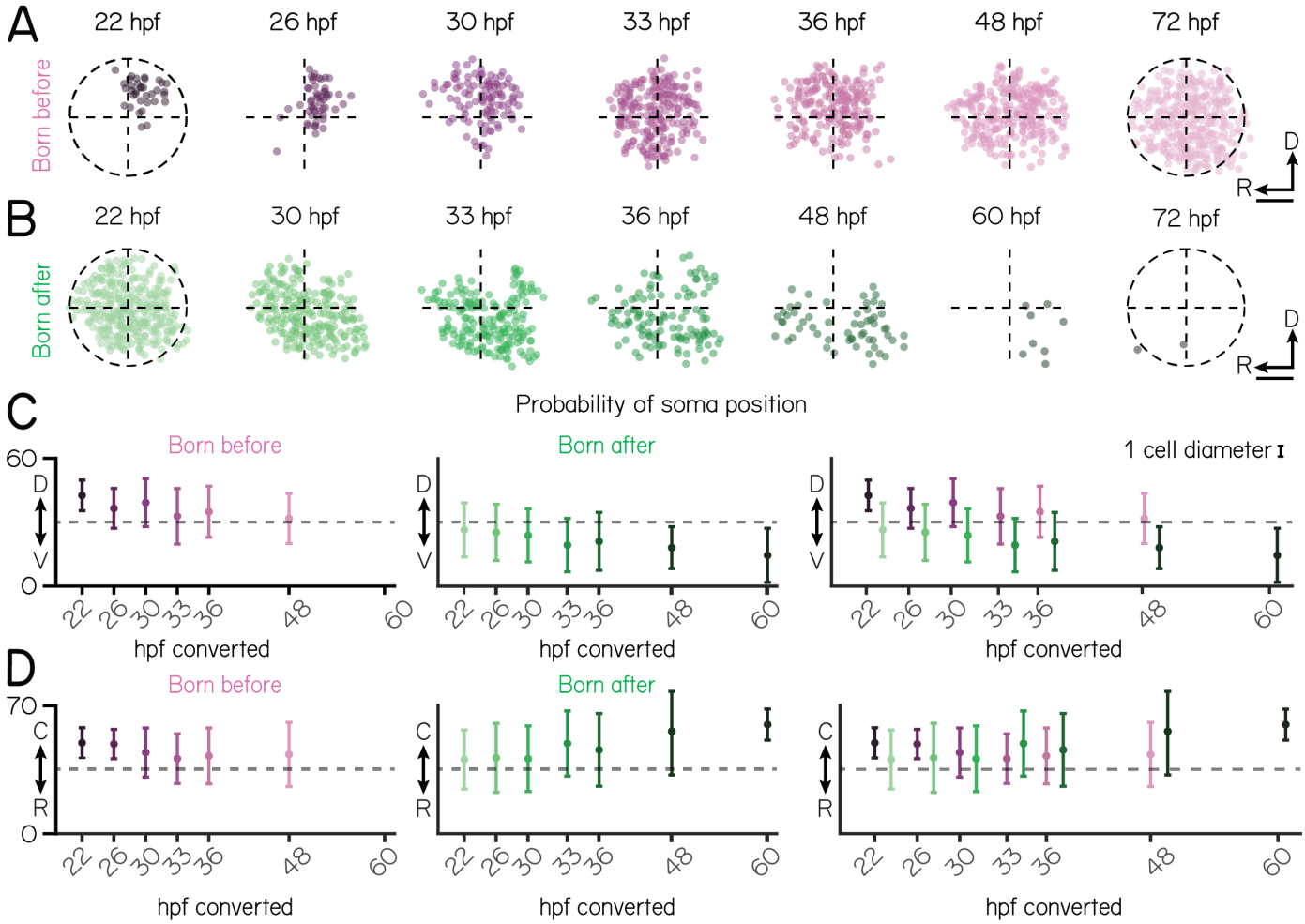

Figure 3: Dorsoventral, but not rostrocaudal development, is the primary predictor of late-born somatic accumulation within the vestibular ganglion.

(A) Soma position of cells born before each timepoint (N=5 fish/timepoint). Dashed horizontal and vertical reference lines indicate the rostrocaudal and dorsoventral midpoints of registered control neurons (Figure 1D).

(B) Soma position of cells born after each timepoint (N=5 fish/timepoint).

(C) Dorsoventral position of neurons born before (magenta) or after (green) each timepoint, shown as median/standard deviation across aggregated data. Horizontal dashed line shows the midpoint.

(D) Rostrocaudal position of neurons born before/after each timepoint, shown as the median/standard deviation across aggregated data.

All scale bars, 20μm except where noted. Full statistics are shown in Table 2.

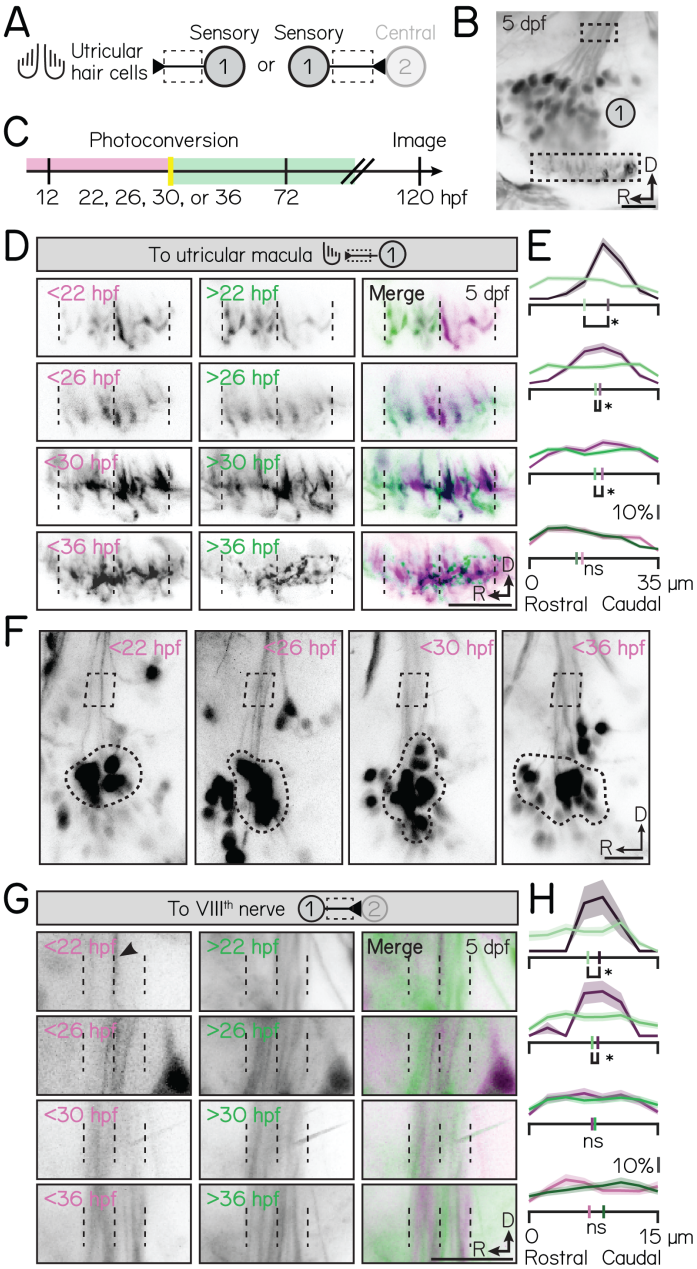

Figure 4: The development of bipolar afferents to local utricular targets and the VIIIth nerve mirrors somatic topography.
(A) Circuit schematic. Black dashed lines outline the circuit elements of focus.
(B) Representative image of the vestibular ganglion, visualized using *Tg(-6.7Tru.Hcrtr2:GAL4-VP16);Tg(UAS-E1b:Kaede)*. Dashed and dotted rectangles outline bipolar afferents to the utricular macula and VIIIth nerve, respectively.
(C) Timeline of birthdating experiments. Larvae were converted at only one timepoint (22, 26, 30, or 36 hpf) and imaged at 5 dpf.
(D) Vestibular ganglion projections to the utricular macula at four converted timepoints (left, converted Kaede; middle, unconverted Kaede; right, merge). As neurons continue to generate new, uncoverted (green) Kaede after the time of conversion, unconverted Kaede projections may originate from both "born before" and "born after" neurons. Black dashed vertical line shows the approximate rostrocaudal extent and midpoint of macula projections based on total unconverted fluorescence (all projections). Data from one example fish/timepoint shown.
(E) Probability of observing converted Kaede (magenta) along the rostrocaudal axis. Each distribution corresponds with the timepoint shown to the left (Figure 4D). Green shows the probability of observing unconverted Kaede, which is not exclusive to "born after" projections (see above). N=3 larvae quantified per timepoint.
(F) Projections to the VIIIth nerve from converted vestibular ganglion soma. Dashed boxes outline the area of the projection bundle quantified in Figure 4G. Dashed circular outline shows soma that were born before the converted timepoint and were above thresholded background levels (Methods). Non-converted, below-threshold soma fluorescence is an artifact of manual brightness adjustment to visualize the fainter projection bundle.
(G) Zoom on VIIIth nerve projections. Black arrow highlights a faint but visibly converted projection converted at 22 hpf. Black dashed lines show the rostrocaudal extent and midpoint, respectively. Data from one example fish/timepoint shown.
(H) Probability of observing converted (magenta) or unconverted (green) Kaede fluorescence along the rostrocaudal axis for each timepoint shown in Figure 4G.
All scale bars, 20 µm. Stars indicate significance at the $p<0.05$ level; n.s., not significant.

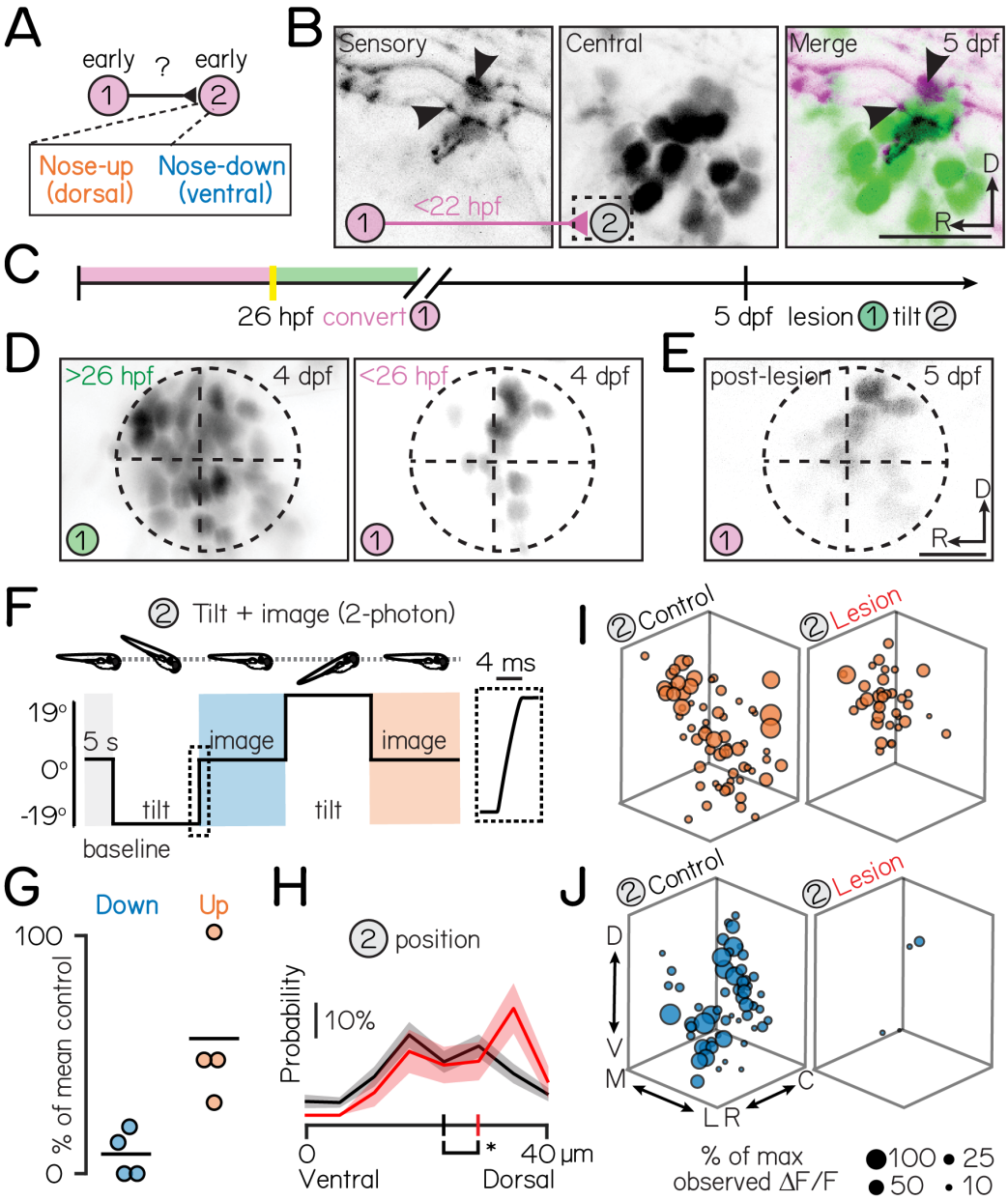

Figure 5: Early-born vestibular ganglion neurons assemble with spatiotemporally-matched central partners in the hindbrain.

(A) Circuit schematic, highlighting the experimental hypothesis and the spatial organization of two directional subtypes (nose-up/nose-down) of central projection neurons.

(B) VIIIth nerve axons from neurons born before 22 hpf (left; magenta) at the central projection neurons in the tangential nucleus (middle; green). Inset (lower right) shows circuit schematic. White arrows point to VIIIth nerve innervation of the dorsal central projection nucleus. Neurons and projections are visualized using *Tg(-6.7Tru.Hcrtr2:GAL4-VP16);Tg(UAS-E1b:Kaede)*.

(C) Timeline of birthdating, lesion, and tilt experiments. Larvae are converted at 26 hpf. At 5 dpf, converted vestibular ganglion neurons are lesioned. Central projection neurons are imaged following tilt stimulation and express *Tg(-6.7Tru.Hcrtr2:GAL4-VP16);Tg(UAS-E1b:Kaede);Tg(UAS:GCaMP6s)*.

(D) Representative images of vestibular ganglion neurons born after (top) or before (bottom) 26 hpf, prior to lesion. Circle and dashed lines outline the vestibular ganglion and spatial midpoints, as shown in Figure 1D. The "born before 26 hpf" image shown was thresholded to subtract background conversion (Methods).

(E) The same larvae shown in Figure 4D after lesioning all but the earliest-born (before 26 hpf) neurons.

(F) Schematic of Tilt In Place Microscopy stimulation and two-photocon calcium imaging paradigm. Shaded bars show imaging periods for baseline (grey), return from nose-down tilt (blue), and return from nose-up tilt (orange). Periods between shaded bars show time when the larvae is tilted away from the imaging plane. Inset shows timecourse of restoration step to horizontal.

(G) Change in the number of nose-up and nose-down neurons measured following lesion of vestibular ganglion neurons born after 26 hpf, quantified as a percentage of the mean number of up/down neurons measured across N=4 control larvae. Each circle is a unique larvae.

(H) Distribution of central neuron somata in the dorsoventral axis in control (grey) and lesioned (red) larvae shown in Figure 5G.

(I) Location of all mapped nose-up central neurons in control and lesioned larve. Each circle is an individual cell, pseudosized by the magnitude of calcium fluorescence change following tilts.

(J) Location of all mapped nose-down central neurons.

All scale bars, 20 µm. Stars denote significance at the p<0.05 level.

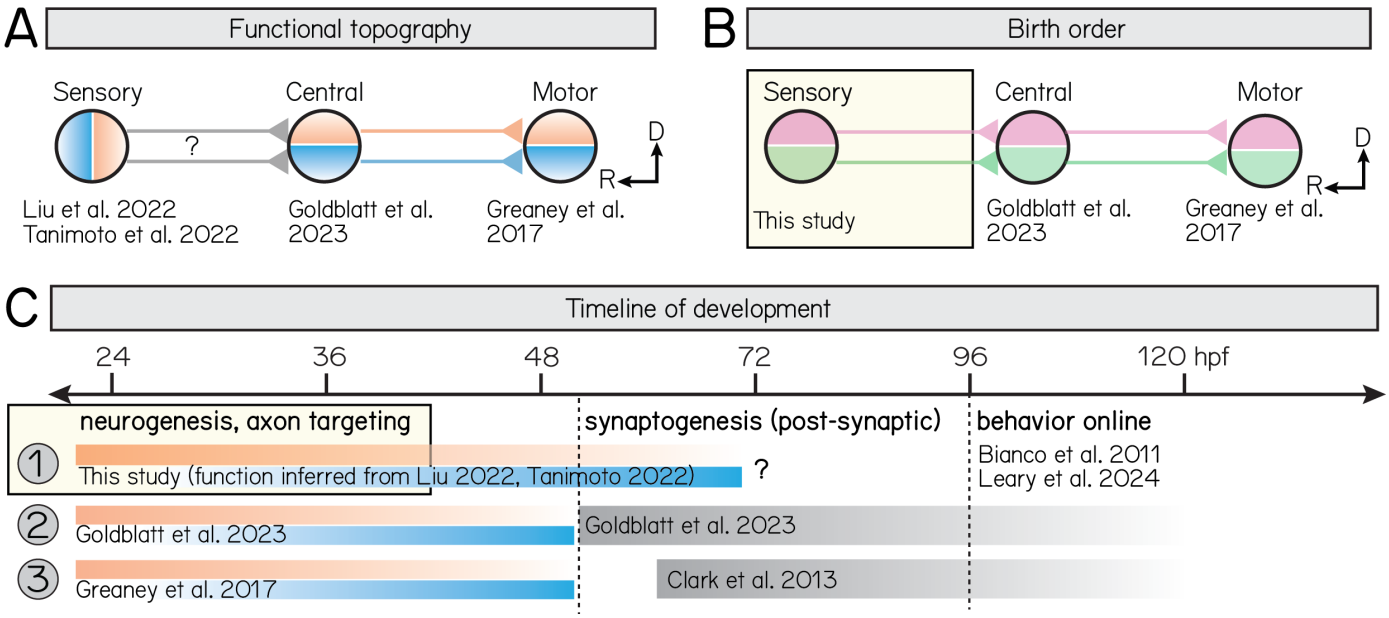

Figure 6: Birth order unifies vestibulo-ocular reflex circuit organization.
(A) Functional topography for each vestibulo-ocular reflex circuit population, adapted from [24–27]. Orange and blue represent nose-up and nose-down domains for each nucleus (circles) and their axonal projections (horizontal lines).
(B) Birth order-related organization of each circuit population, adapted from [26,27] and findings from the present study. Magenta and green represent early- and late-born cohorts, respectively. Yellow box highlights the advances from the present study.
(C) Timeline of key developmental events for each circuit population in zebrafish. Data is from this study and [26,27,36,37,71]. Yellow box highlights the advances from the present study. Up/down function in the vestibular ganglion is inferred based on correlations between anatomical position (this study) and functional topography [24,25]. The timecourse of sensory-central synaptogenesis has not been determined in zebrafish.

Age converted	# cells/fish, born before	approx. % of control, born before	# cells/fish born after
22	7±2	9%	59±7
26	11±2	14%	49±7
30	21±2	27%	44±5
33	42±2	55%	36±5
36	40±5	52%	22±4
48	52±8	68%	12±2
60	n/a		3±1
72	63±5	82%	0.5±0.5
Control	77±15		

Table 1: Number of statoacoustic ganglion neurons converted across developmental timepoints. Data shown as mean/std number of neurons born before or after each timepoint from N=5 hemispheres/timepoint. Control refers to neurons from N=5 larvae from *Tg(-6.7Tru.Hcrtr2:VP16-GAL4);Tg(UAS-E1b:Kaede)* (Figure 1D).

Age converted	Median position born before (µm)	Median position born after (µm)	$p_{KS\ test}$ born before vs. born after	$p_{ANOVA,\ mult\ compare}$ born before vs. prev. age	$p_{ANOVA,\ mult\ compare}$ born after vs. prev. age
Dorsoventral					
22	17.3±7.2	33.5±12.7	9.9E-10		
26	23.4±9.4	34.7±13.3	7.6E-07	0.50	0.99
30	20.7±11.3	36.1±12.5	2.3E-12	0.99	0.80
33	27.1±13.1	40.7±12.5	9.0E-09	5.2E-05	0.08
36	25.0±12.0	38.9±13.6	2.2E-11	0.20	0.97
48	28.2±11.8	41.9±9.9	7.2E-09	0.18	0.34
60	n/a	45.5±12.7	n/a		0.99
72	34.5±13.9	53.3±2.0	0.04		0.99
Rostrocaudal					
22	42.7±7.1	34.9±13.9	7.6E-06		
26	42.2±6.9	35.7±16.2	2.2E-08	0.99	0.99
30	38.2±11.5	35.3±15.4	0.08	0.10	0.99
33	35.3±11.7	42.4±15.3	6.6E-07	0.94	0.48
36	36.6±13.2	39.4±17.1	1.1E-04	0.99	0.99
48	37.2±15.1	48.2±20.6	7.9E-04	0.97	0.99
60	n/a	51.3±7.3	n/a		0.66
72	38.2±14.1	21.8±17.1	0.28		0.24
Mediolateral					
22	3.0±0.6	3.0±0.9	0.01		
26	3.0±0.8	3.0±1.0	0.03	0.99	0.99
30	3.0±0.9	3.0±1.0	.99	0.04	0.99
33	3.0±0.9	3.0±0.9	0.01	0.99	0.48
36	3.0±0.9	3.0±0.9	0.06	0.99	0.99
48	3.0±0.8	3.0±0.9	0.52	0.97	0.99
60		3.0±0.5			0.66
72	3.0±0.9	2.5±0.7	0.73		0.24

Table 2: Statistical comparisons of temporal cohort somatic organization. Median (standard deviation) positions are shown as microns from the dorsal- or rostral-most edges (0 µm) of the vestibular ganglion. Data is shown as an aggregate of all neurons mapped across N=5 hemispheres/timepoint.